Parameter Degeneracy in Flavor-Dependent Reconstruction of Supernova Neutrino Fluxes

Hisakazu Minakata[1],[*] Hiroshi Nunokawa[2],[†] Ricard Tomàs[3‡],[§] and Jose W. F. Valle[3¶]

[1]*Department of Physics, Tokyo Metropolitan University, Hachioji, Tokyo 192-0397, Japan*

[2]*Departamento de Física, Pontifícia Universidade Católica do Rio de Janeiro,*

C. P. 38071, 22452-970, Rio de Janeiro, Brazil

[3]*AHEP Group, Institut de Física Corpuscular – C.S.I.C.,*

Universitat de València, Edifici Instituts d'Investigació,

Apt. 22085, E–46071 València, Spain

(Dated: February 15, 2008)

Abstract

We reexamine the possibility of reconstructing the initial fluxes of supernova neutrinos emitted in a future core-collapse galactic supernova explosion and detected in a Megaton-sized water Cherenkov detector. A novel key element in our method is the inclusion, in addition to the total and the average energies of each neutrino species, of a "pinching" parameter characterizing the width of the distribution as a fit parameter. We uncover in this case a continuous degeneracy in the reconstructed parameters of supernova neutrino fluxes at the neutrinosphere. We analyze in detail the features of this degeneracy and show how it occurs irrespective of the parametrization used for the distribution function. Given that this degeneracy is real we briefly comment on possible steps towards resolving it, which necessarily requires going beyond the setting presented here.

PACS numbers: 14.60.Lm,14.60.Pq,97.60.Bw

‡ Present address: II. Institut für Theoretische Physik, Universität Hamburg, Luruper Chaussee 149, 22761 Hamburg, Germany

[*]Electronic address: minakata@phys.metro-u.ac.jp

[†]Electronic address: nunokawa@fis.puc-rio.br

[§]Electronic address: ricard.tomas.bayo@desy.de

[¶]Electronic address: valle@ific.uv.es

Typeset by REVTEX

1

I. INTRODUCTION

The detection of neutrinos from the SN1987A by the Kamiokande [1, 2] and IMB [3] collaborations not only confirmed the basic picture of the core collapse supernovae (SN) but also initiated a whole new field of observational supernova astrophysics. In fact, the observation of SN neutrinos is the unique way, except possibly for gravitational wave detection, to directly probe into the interior of a star which is undergoing gravitational collapse. Despite this pioneering observation, a precise understanding of the physics of a SN explosion still eludes us. Spherically symmetric models of iron core collapse do not explode, even with solid neutrino transport [4, 5, 6] and general relativity [7]. In the two-dimensional models the outcomes vary qualitatively and quantitatively [8, 9, 10, 11], reflecting the increased complexity of the physics involved.

Owing to their feeble interactions, neutrinos are able to escape from deep inside the star. Therefore SN neutrinos can provide us with information about the highly dense inner layers, where the SN explosion is initiated. Moreover, the composition of the SN core is such that the reactions involved in the creation and annihilation of neutrinos are different for the different neutrino flavors. These differences are imprinted in the emerging neutrino fluxes. These are non-thermal and can be characterized by the total energy emitted, the mean energy and the so-called *pinching* parameter which controls the width of the distribution. Therefore, a flavor-dependent reconstruction of SN neutrino flux is a useful probe for diagnosing SN core. (For early references, see e.g., [12].) The physics which can be probed would include that governing matter under extreme conditions, such as information about the equation of state, and the explosion mechanism itself [13].

The potential of neutrinos in probing the SN core results, on the one hand, from the huge flux of them that will be released, corresponding to around 99 % of the total energy emitted in the SN explosion. On the other hand it is helped (though it may sound ironic) by the flavor mixing properties of neutrinos, including the large "solar" neutrino mixing angle obtained by KamLAND [14] and the solar neutrino observation, in particular, SNO [15]. For an updated global analysis of the data of the various neutrino oscillation experiments, see e.g., [16, 17].

If a supernova explosion takes place in our galaxy the number of neutrino events expected in the current and planned neutrino detectors will be enormous [18, 19]. Among all neutrino detectors water Cherenkov detectors are most likely the ones which can run long enough to watch galactic SN over long enough time scales. It is therefore important to establish a strategy for diagnosing the core of SN by using neutrino observation by water Cherenkov detectors.

Inverse beta decay $\bar{\nu}_e + p \to e^+ + n$ provides the main neutrino detection reaction in such a detector. According to the standard picture of supernova neutrino propagation, except for the case of inverted mass hierarchy and large θ_{13} ($\sin^2 \theta_{13} \gtrsim 10^{-3}$), the energy spectrum of $\bar{\nu}_e$ at the Earth is expected to be a strong mixture of the original $\bar{\nu}_e$ and ν_x (we collectively denote ν_μ, ν_τ, $\bar{\nu}_\mu$, $\bar{\nu}_\tau$ as ν_x since at first approximation their properties are identical and can be treated as a single species), modulated by the large value of solar mixing angle, θ_{12}, well determined by solar and KamLAND data [16, 17]. By performing a suitable simulation of the high-statistics SN data it was shown in Refs. [20, 21] how one can determine the parameters of the original neutrino spectra, $\bar{\nu}_e$ and ν_x in terms of the $\bar{\nu}_e$ signal detected in inverse beta decay. However, this result has been obtained under the assumption that we know the parameter which describes the "pinching" of the SN neutrino fluxes. (See Sec. II A for the pinching.)

In this paper, we extend our previous work in [20] by including the pinching of the SN neutrino spectra as fit parameters[1]. In the extended framework, regrettably enough, we face with an important difficulty in reconstructing the original neutrino spectra. Most significantly, we find that there exists a persistent continuous degeneracy in the flavor-dependent determination of the luminosity and the spectra of SN neutrinos.

In order to make our point and to indicate how serious the degeneracy problem is, we show in Fig. 1 examples of two degenerate $\bar{\nu}_e$ energy spectra at the Earth (upper panels) as well as their difference divided by the true spectrum or fractional difference (lower panels) for two different parametrizations of the SN neutrino flux. It is remarkable that, despite the large difference in the primary neutrino spectra at the SN core particularly for ν_x, the true and fake spectra agree with each other within better than 1% level over a wide energy range. It is evident that the degeneracy is present already in the bare neutrino fluxes reaching the detector (before taking into account experimental uncertainties such as energy resolution) and it looks so perfect that it is unlikely to be resolved even with the extremely high statistics expected in a Megaton detector [24, 25, 26]. Hopefully, our negative result will stimulate further studies towards a full diagnosis of the SN core by neutrino observations. These include a better theoretical understanding of the neutrino fluxes formation, as well as an optimization of the information provided by the different reactions in the neutrino detectors.

The plan of the paper is as follows. In Sec. II we describe the basic features of supernova neutrinos, including the different parametrizations of the initial neutrino spectra usually considered in the literature, as well as the effect of neutrino flavor conversion before reaching

---

[1] A study of the relevance of this parameter in the analysis of the neutrino signal from SN1987A can be found for instance in Refs. [22, 23].
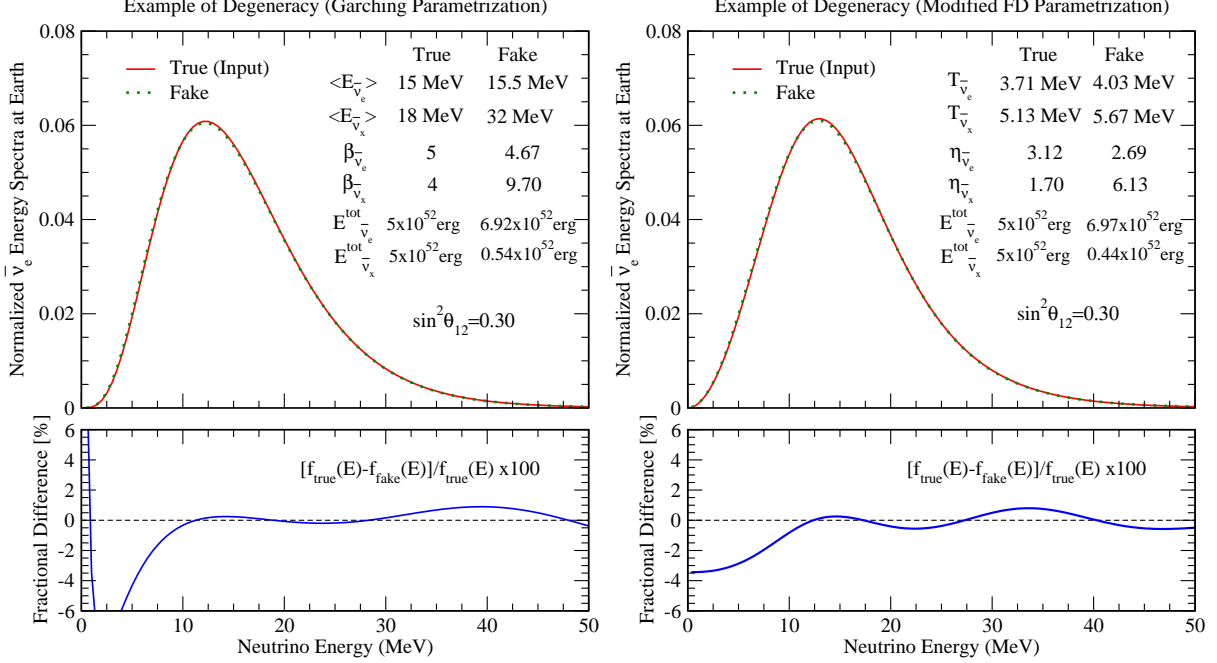
FIG. 1: Examples of degenerate determination of SN astrophysical parameters. The two degenerate neutrino energy spectra at Earth (upper panels) as well as their fractional difference (lower panels) resulting from neutrino fluxes with two different energy spectra at the SN core and the indicated parameter sets. The left and right panels correspond to the Garching parametrization and the modified Fermi-Dirac parametrization, respectively. Input values are the same ones shown in Table I. While it is not clear from the legend in the right panel, we note that the both true and fake values of average energies for the Fermi-Dirac parametrization give the same values as in the case of Garching one. Normal neutrino mass hierarchy has been assumed. Notations of neutrino species and the definitions of the parameters involved are given in Sec. II.

the detector. In Sec. III we will specify the assumptions used in our analysis. Those include the particular values characterizing the initial neutrino fluxes, the details of the detector, and the neutrino mass scheme. In Sec. IV we demonstrate the existence of a continuous degeneracy in the determination of the astrophysical parameters. We discuss the robustness of this finding, which results neither from the particular parametrization taken, nor from a particular set of SN parameters. Finally, in Sec. V we speculate possible ways that could help overcoming the degeneracy problem.

4

II. SUPERNOVA NEUTRINOS

A. Basic features of neutrino spectra from supernova

To a crude approximation the proto-neutron star is a black-body source for neutrinos of all flavors. For the case of ν_e and $\bar{\nu}_e$ the dominant reactions are the charged-current (CC) interactions with nucleons $e^- + p \leftrightarrow \nu_e + n$ and $e^+ + n \leftrightarrow \bar{\nu}_e + p$. The other flavors, ν_μ, $\bar{\nu}_\mu$, ν_τ, $\bar{\nu}_\tau$ which in this paper we shall collectively denote by ν_x, interact with the surrounding matter via neutral current (NC) interactions, e.g. Bremsstrahlung, neutrino-pair annihilation or neutrino-nucleon scattering. These processes keep ν_e, $\bar{\nu}_e$ and ν_x in local thermal equilibrium up to the radii where these reactions become inefficient (neutrinosphere). Beyond these radii neutrinos freely stream. Taking into account the hierarchy in the cross sections, $\sigma_{CC} > \sigma_{NC}$ as well as the richer neutron composition than protons, one expects the average neutrinosphere radii of ν_x, $\bar{\nu}_e$, and ν_e to obey $r_x < r_{\bar{e}} < r_e$, so that ν_x (ν_e) decouples at the highest (lowest) temperature. This translates to an ordering of the average energies of SN neutrinos $\langle E_{\nu_e} \rangle < \langle E_{\bar{\nu}_e} \rangle < \langle E_{\nu_x} \rangle$, the exact degree of difference still under debate [27, 28, 29]. See, for example, [30, 31] for more about physics in the proto-neutron star.

The location of the neutrinospheres does not only depend on the neutrino flavor but also on its energy. The energy dependence of the cross sections of the processes involved makes neutrinos with different energies decouple from the proto-neutron star at different radii and therefore different local temperatures. For this reason the spectrum of the neutrinos leaving the star does not present a thermal distribution. The possibility of reconstructing the flux parameters of the three effective flavors from observation would lead to a "neutrino imaging" of the proto-neutron star.

There are different ways to characterize the non-thermal spectra of the neutrino fluxes emerging from the SN. Among them there are two parametrizations that have been extensively used in the literature. One is the Fermi-Dirac distribution motivated by the equilibrium distribution of neutrinos inside the star [22]

$$F_{\nu_\alpha}^0(E) = \frac{\Phi_{\nu_\alpha}}{T_{\nu_\alpha}^3 f_2(\eta_{\nu_\alpha})} \frac{E^2}{e^{E/T_{\nu_\alpha} - \eta_{\nu_\alpha}} + 1}, \tag{1}$$

where E is the neutrino energy, and T_{ν_α} and η_{ν_α} denote an effective temperature and degeneracy parameter (chemical potential), respectively. The distribution is normalized so that Φ_{ν_α} stands for the total number of ν_α emitted. The function $f_n(\eta_{\nu_\alpha})$ is defined as

$$f_n(\eta_{\nu_\alpha}) \equiv \int_0^\infty \frac{x^n}{e^{x - \eta_{\nu_\alpha}} + 1} \mathrm{d}x \,. \tag{2}$$

5

The mean energy and the total energy released are consequently $\langle E_{\nu_\alpha} \rangle = [f_3(\eta_{\nu_\alpha})/f_2(\eta_{\nu_\alpha})] T_{\nu_\alpha}$ and $E_{\nu_\alpha}^{\text{tot}} = \Phi_{\nu_\alpha} \langle E_{\nu_\alpha} \rangle$, respectively. Note that it must be understood that Φ_{ν_x} does not refer to the sum of the flux of the non-electron species (despite that we treat them as a single species) but the individual one as follows,

$$\Phi_{\nu_x} = \Phi_{\nu_\mu} = \Phi_{\bar{\nu}_\mu} = \Phi_{\nu_\tau} = \Phi_{\bar{\nu}_\tau}, \tag{3}$$

and so as for $E_{\nu_x}^{\text{tot}}$, throughout this paper.

A way to determine how much a spectrum deviates from being thermal is to use the pinching parameter [27] defined as the ratio of the first two moments

$$p \equiv \frac{\langle E^2 \rangle}{\langle E \rangle^2}. \tag{4}$$

A spectrum that is thermal up to its second moment has $p = p_{\text{FD},\eta=0} \approx 1.3029$, while $p < p_{\text{FD},\eta=0}$ implies a pinched spectrum (high- and low-energy parts of the spectrum relatively suppressed) and $p > p_{\text{FD},\eta=0}$ is an anti-pinched spectrum (high- and low-energy parts of the spectrum enhanced). For the Fermi-Dirac distribution with an arbitrary η the pinching parameter p is related to η as

$$p = [f_4(\eta) f_2(\eta)/f_3^2(\eta)]$$

. In the left panel of Fig. 2 we show in solid red lines the explicit dependence of the pinching parameter on the effective degeneracy parameter η.

The curve becomes flat at negative η, which reflects the fact that the function tends to the Maxwell-Boltzmann spectrum at $\eta \to -\infty$, which does not differ much from the Fermi-Dirac one, $\eta = 0$. In dashed lines we present the strong dependence of $\langle E \rangle / T$ on η for pinched distributions.

A second parametrization using the form of power times exponential has been recently introduced by the Garching group as a better parametrization of their simulation results [28, 30, 32]

$$F_{\nu_\alpha}^0(E) = \frac{\Phi_{\nu_\alpha}}{\langle E_{\nu_\alpha} \rangle} \frac{\beta_{\nu_\alpha}^{\beta_{\nu_\alpha}}}{\Gamma(\beta_{\nu_\alpha})} \left(\frac{E}{\langle E_{\nu_\alpha} \rangle} \right)^{\beta_{\nu_\alpha}-1} \exp\left(-\beta_{\nu_\alpha} \frac{E}{\langle E_{\nu_\alpha} \rangle} \right). \tag{5}$$

In this case the parameters characterizing the distribution function are the total number of ν_α emitted, Φ_{ν_α}, the mean energy, $\langle E_{\nu_\alpha} \rangle$, and a parameter β_{ν_α} which is related to the pinching parameter via

$$p = (\beta_{\nu_\alpha} + 1)/\beta_{\nu_\alpha}.$$

In the right panel of Fig. 2 we show in solid red lines the dependence of p on β_{ν_α}. In contrast to the Fermi-Dirac parametrization there is no asymptotic limit for the width $\langle E^2 \rangle / \langle E \rangle^2$,
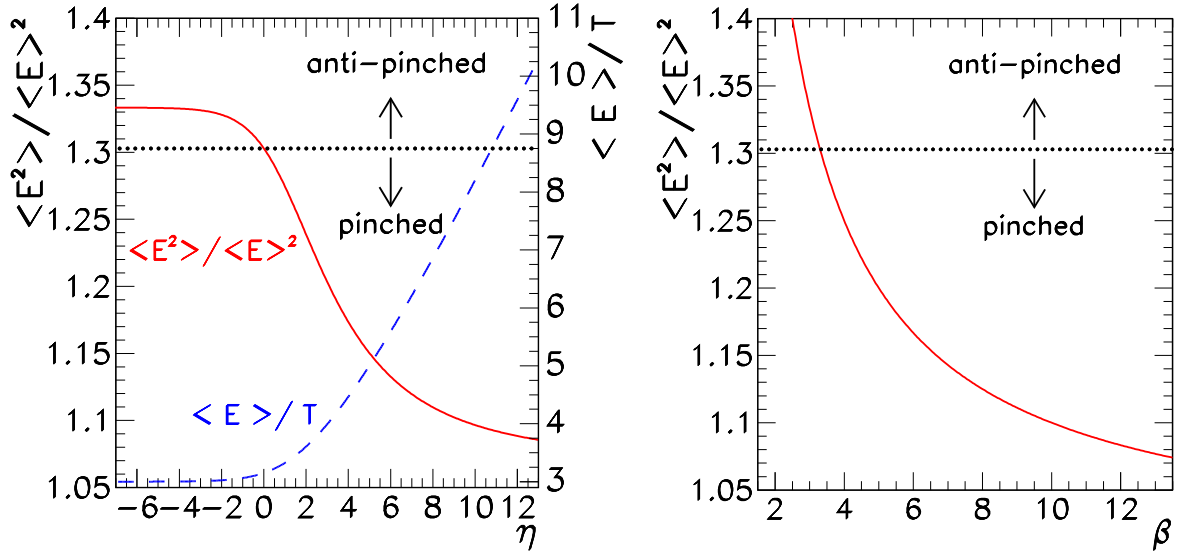
FIG. 2: The Left panel gives the pinching parameter $p \equiv \langle E^2 \rangle / \langle E \rangle^2$ (left label) and the ratio $\langle E \rangle / T$ (right label) for the Fermi-Dirac distribution represented as a function of η by the solid and dashed curves, respectively. The critical value of p which separates between a pinched and an anti-pinched distribution is indicated by the dotted line. The right panel gives the pinching parameter for the Garching parametrization as a function of β.

hence this parametrization can reproduce better anti-pinched distributions. In Fig. 3 we illustrate the effect of the pinching on three spectra with different β's. One can see how the pinched spectrum is suppressed at low and high energies with respect to the non-pinched one. This in turn shows a similar suppression in comparison with the anti-pinched spectrum. We observe in the same figure how this behavior holds also for the case of the Fermi-Dirac distributions. The results shown above agree with those found in [30] where the similarities as well as differences of these 2 parametrizations were explored.

B. Flavor conversion of supernova neutrinos

The dynamics of neutrino flavor conversion in a typical iron-core SN can be factorized into two different parts [2]: the propagation through the inner layers, where the high neutrino

---

[2] There are also particular scenarios with very shallow electron density profiles, like the early stages of O-Ne-Mg core SNe [33], where the dynamics in the inner and outer regions can not be decoupled. In this case collective effects and MSW resonances are not clearly separated, what can lead to interference effects both in normal and inverted mass hierarchy [34]. In the following, though, we will not consider this particular case.
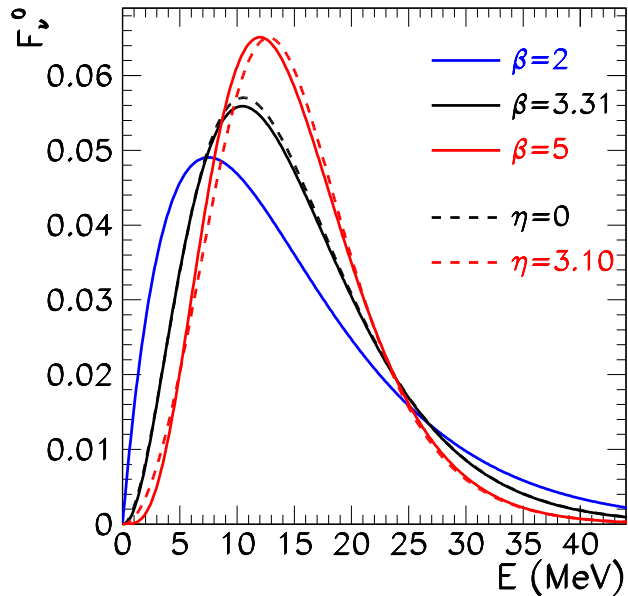
FIG. 3: The solid curves show examples of anti-pinched ($\beta = 2$, shown in blue), un-pinched ($\beta = 3.31$, in black), and pinched ($\beta = 5$, in red) Garching distributions normalized to unity. The mean energy has been set to 15 MeV. The corresponding Fermi-Dirac distributions for the same value of $\langle E \rangle$ and p are also shown by the dashed lines. Note that there is essentially no anti-pinched Fermi-Dirac distribution for $\beta = 2$ because of the saturation property of p shown in Fig. 2.

density can lead to non-linear collective effects [34, 35, 36, 37, 38, 39, 40, 41, 42, 43, 44], and the evolution in the outer layers. Right above the neutrinosphere the neutrino density is so high that neutrino-neutrino interactions must be taken into account. The presence of neutrino self-interactions potentially give rise to collective phenomena on the neutrino propagation. These include synchronization, pair conversions of the kind $\nu_e \bar{\nu}_e \to \nu_x \bar{\nu}_x$ during the so-called bipolar regime, and spectral split. These effects, though, arise only in the case of inverted neutrino mass hierarchy.

In the outer layers the neutrino-neutrino interactions can be neglected and therefore it is enough to consider the Mikheev-Smirnov-Wolfenstein (MSW) effects induced on neutrinos by background matter [45, 46]. The neutrino flavor evolution can be then described in terms of two independent two-level crossings associated to the atmospheric and solar mass squared splittings [47, 48]. Let us denote the former (latter) the H (L) level crossing. The relation is simplified by the fact that the L level crossing is adiabatic, given the confirmation of the large mixing angle solution by the KamLAND data.

Yet, there are still uncertainties which arise due to the two remaining unknowns, the neutrino mass hierarchy and the value of θ_{13}. The former leads to the freedom of the H level crossing in either the neutrino or the anti-neutrino channels depending upon the normal or

Flux model	average energy ($\bar{\nu}_e$)	average energy (ν_x)	pinching ($\bar{\nu}_e$)	pinching (ν_x)
Garching	$\langle E_{\bar{\nu}_e} \rangle = 15$ MeV	$\langle E_{\nu_x} \rangle = 18$ MeV	$\beta = 5$	$\beta = 4$
Fermi-Dirac	$T_{\bar{\nu}_e} = 3.71$ MeV	$T_{\nu_x} = 5.13$ MeV	$\eta = 3.12$	$\eta = 1.70$

TABLE I: Reference input values of the Garching and the Fermi-Dirac flux parameters used in this work. The total energies and the width $\langle E^2 \rangle / \langle E \rangle^2$ of $\bar{\nu}_e$ and ν_x are taken as follows: $E_{\bar{\nu}_e}^{\rm tot} = E_{\nu_x}^{\rm tot} = 5 \times 10^{52}$ erg, $p_{\bar{\nu}_e} = \langle E_{\bar{\nu}_e}^2 \rangle / \langle E_{\bar{\nu}_e} \rangle^2 = 1.2$, and $p_{\bar{\nu}_x} = \langle E_{\nu_x}^2 \rangle / \langle E_{\nu_x} \rangle^2 = 1.25$. The flux Φ_{ν_α} is determined by the relation $E_{\nu_\alpha}^{\rm tot} = \Phi_{\nu_\alpha} \langle E_{\nu_\alpha} \rangle$. The temperatures and the η_{ν_α} of the Fermi-Dirac distribution are chosen to reproduce the same average energies listed in the upper row and the same p.

the inverted mass hierarchies, respectively, which in principle can be used to discriminate the hierarchy [48, 49, 50, 51, 52, 53, 54, 55, 56]. The latter allows the possibilities of the adiabatic or the non-adiabatic H level crossing depending upon $\sin^2 \theta_{13} \gtrsim 10^{-3}$ or $\sin^2 \theta_{13} \lesssim 10^{-5}$.

III. ASSUMPTIONS

A. SN flux model

We employ a SN model-dependent fitting method to reconstruct SN neutrino fluxes at the core. We trust global features of the SN neutrino fluxes at the core obtained by detailed simulations and parametrize them by simple functions. We adopt two choices, namely, the traditional Fermi-Dirac form Eq. (1) and the Garching parametrization in Eq. (5). Both parametrizations contain three parameters, $(\Phi_{\nu_\alpha}, \langle E_{\nu_\alpha} \rangle, \beta_{\nu_\alpha})$ and $(\Phi_{\nu_\alpha}, T_{\nu_\alpha}, \eta_{\nu_\alpha})$ for the Garching and the Fermi-Dirac distributions, respectively. In previous works [20, 21, 56, 57] the pinching parameters were always fixed and thus assumed to be known in advance. The inclusion of β_{ν_α} (η_{ν_α}) parameter as a fit parameter constitutes therefore a new feature of the present analysis. We feel that this inclusion is essential because the pinching parameter represents the effect of departure from local thermal equilibrium and would reflect the environmental condition of matter around the neutrinosphere. Hence, it should be determined by observations. The values of initial parameters used to generate SN neutrino "data" are summarized in Table I. We assume that SN neutrino spectra are time-independent during the burst. Although this may be too idealized, it is a conservative assumption in the sense that relaxing this it would further complicate the task of resolving the degeneracy.

B. Detector and analysis method

In this paper, we focus on water Cherenkov detectors as they are most likely the ones to run sufficiently long so as to watch galactic supernovae over long enough time scales. In particular we consider Hyper-Kamiokande [24], and take the fiducial mass of 720 kton assuming that the whole inner volume is available for SN neutrinos. For other similar projects see e.g. Refs. [25, 26].

In this kind of detectors several reactions contribute to the SN neutrino signal: inverse beta decay, elastic scattering off electrons, and CC and NC with oxygen. Nevertheless, inverse beta decay is indeed the dominant reaction, which would yield $\sim 2 \times 10^5$ events in Hyper-Kamiokande for a SN at 10 kpc from the Earth. For the cross section see Ref. [58, 59]. The expected event numbers from ν_e and ν_x elastic scattering and ν_e absorption by Oxygen are more than an order of magnitude below [18].

In this paper, thus, we restrict our analysis into a unique observable, the positron energy spectra produced by the $\bar{\nu}_e$ absorption reaction on protons, $\bar{\nu}_e + p \rightarrow e^+ + n$. For this reaction only six parameters are relevant: $E_{\bar{\nu}_e}^{\mathrm{tot}}$, $\langle E_{\bar{\nu}_e} \rangle$, $p_{\bar{\nu}_e} \equiv \langle E_{\bar{\nu}_e}^2 \rangle / \langle E_{\bar{\nu}_e} \rangle^2$, $E_{\nu_x}^{\mathrm{tot}}$, $\langle E_{\nu_x} \rangle$, and $p_{\nu_x} \equiv \langle E_{\nu_x}^2 \rangle / \langle E_{\nu_x} \rangle^2$. We assume the SN at a distance of 10 kpc from the Earth and generate the SN neutrino flux data by assuming the seed parameters listed in Table I. The data are subsequently fitted using the same parametrization assumed to generate it, except for results shown in Fig. 9. Motivated by our current understanding of the composition of the proto-neutron star we also assume that the ratio [3] $\tau \equiv \langle E_{\nu_x} \rangle / \langle E_{\bar{\nu}_e} \rangle > 1$. We perform a standard χ^2 analysis including only the statistical error. The energy bins used are chosen as: 70 bins for $5\mathrm{MeV} \leq E_e \leq 40\mathrm{MeV}$, 10 bins for $40\mathrm{MeV} \leq E_e \leq 50\mathrm{MeV}$, 3 bins for $50\mathrm{MeV} \leq E_e \leq 56\mathrm{MeV}$, 1 bin for $56\mathrm{MeV} \leq E_e \leq 60\mathrm{MeV}$, and the highest energy bin for $60\mathrm{MeV} \leq E_e \leq 100\mathrm{MeV}$ (total 85 bins), where E_e stands for the measured energy of the positrons. The energy resolution is taken into account with a Gaussian function with width $\sigma_{\mathrm{res}} = 0.47\sqrt{E_e/\mathrm{MeV}}$ MeV, following Ref. [60]. The results are represented in terms of $E_{\nu_\alpha}^{\mathrm{tot}}$, $\langle E_{\nu_\alpha} \rangle$ and $\langle E_{\nu_\alpha}^2 \rangle / \langle E_{\nu_\alpha} \rangle^2$. The 2 (3) σ CL allowed regions are determined by the condition,

$$\Delta\chi^2 = \chi^2 - \chi_{\mathrm{min}}^2 < 6.18 \ (11.83), \tag{6}$$

---

[3] To extract the *real degeneracy* we want to eliminate a trivial degeneracy which inevitably comes in into such fitting procedure. In view of Eq. (7) it is clear that for any solution for the six parameters labeled as (a), there is another solution labeled as (b) in which $\beta_{\bar{\nu}_e}^{(b)}$, $\langle E_{\bar{\nu}_e} \rangle^{(b)}$ are replaced by $\beta_{\nu_x}^{(a)}$, and $\langle E_{\nu_x} \rangle^{(a)}$, and vice versa, together with $\Phi_{\bar{\nu}_e}^{(b)} = \tan^2\theta_{12}\Phi_{\bar{\nu}_e}^{(a)}$, $\Phi_{\nu_x}^{(b)} = \cot^2\theta_{12}\Phi_{\nu_x}^{(a)}$. In these expressions, we have used the approximation $s_{13} \ll 1$ for simplicity. We have explicitly verified that the exchange degeneracy solution can be removed by imposing the former condition.

for 2 degrees of freedom.

C.   Neutrino mass hierarchy and validity of our ansatz of SN neutrino flux spectra

In this paper we assume that SN neutrino spectra at the surface of the progenitor star are given by the flavor transformed ones of the initial spectra of either the Garching or the Fermi-Dirac type.

In order to illustrate the possibility of inferring the original neutrino spectra we consider the case with normal mass hierarchy. Ignoring the Earth matter effect, the relationships between the $\bar{\nu}_e$ flux at the core of SN and the one at terrestrial detectors is as follows:

$$F_{\bar{\nu}_e} = c_{12}^2 c_{13}^2 F_{\bar{\nu}_e}^0 + (1 - c_{12}^2 c_{13}^2) F_{\nu_x}^0 \approx c_{12}^2 F_{\bar{\nu}_e}^0 + s_{12}^2 F_{\nu_x}^0 \,, \tag{7}$$

where the expressions s_{12}^2, c_{12}^2, s_{13}^2, and c_{13}^2 stand for $\sin^2 \theta_{12}$, $\cos^2 \theta_{12}$, $\sin^2 \theta_{13}$, and $\cos^2 \theta_{13}$, respectively. The observed $\bar{\nu}_e$ spectra is then a superposition of the original $\bar{\nu}_e$ and ν_x spectra. The coefficients of the composition depend basically on the value of θ_{12}, which we will assume to be $\sin^2 \theta_{12} = 0.3$ [16, 17]. Therefore the goal of the analysis is to disentangle the two different components present in the observed $\bar{\nu}_e$ spectrum.

The validity of our analysis would be affected if any mechanisms are operational inside or outside SN core that invalidate the above ansatz. These include basically three possibilities. The first one is a possible unknown time dependence of the parameters characterizing the initial neutrino fluxes. In this case one can always carry out the analysis for considering the positron spectra at different time bins. The main consequence of this effect will be an increase of the statistical errors but the main features would remain.

The second aspect that could affect our analysis is the presence of the shock waves propagating within the supernova. In several works [61, 62, 63, 64] it has been discussed how the presence of these discontinuities could introduce an energy and time modulation in the survival probabilities. However, the $\bar{\nu}_e$ flux is only affected in the case of inverted mass hierarchy and "large" θ_{13}, $\sin^2 \theta_{13} \gtrsim 10^{-4}$. The formation of shock waves could additionally lead to turbulent density fluctuations, causing a neutrino flavor depolarization as discussed in [65] and [66] where the former considered the δ-correlated density fluctuation whereas the latter considered the Kolmogorov-type turbulence implied by realistic SN simulations. The characteristic signal due to the shock wave, which was originally considered visible ignoring the effects of turbulence and/or density fluctuations, tend to be washed out by such turbulent density fluctuations [65, 66]. See also [67, 68] for effects related to the shock waves. We note, however, that as long as the $\bar{\nu}_e$ flux (at Earth) is concerned, these effects would be significant only in the case of inverted mass hierarchy and not so small value of

θ_{13}, $\sin^2 \theta_{13} \gtrsim O(10^{-3})$.

The third case where our analysis would not apply would be in the presence of decoherence. This can be due to the multi-angle nature of the neutrino self-interaction, and can be present for both normal and inverted mass hierarchies. Nevertheless, it is expected to significantly affect the neutrino propagation only for very similar ν_e and $\bar{\nu}_e$ spectra [40], which does not seem to be the case according to the SN simulations [32]. Therefore we will neglect it.

Last, but not least, the possible existence of non-standard neutrino interactions, apart from affecting neutrino propagation through the SN envelope, could induce resonant conversions in the most deleptonised inner layers [69] with possibly dramatic effects in a Megaton water Cherenkov detector [70]. This possibility will also not be considered here.

Before closing this section let us mention that a similar analysis could be performed in the case of inverted mass hierarchy. However, in this case one should take into account the possible modulations induced by the shock wave passage, as well as by collective effects such as the spectral split in $\bar{\nu}_e$ [42] or the effect of the second-order difference between the ν_μ and ν_τ refractive index [43]. This comparative study lies however beyond the scope of this paper.

IV. DEGENERACY IN FITTED PARAMETERS

A. Continuous degeneracy in the fit parameters

Let us start with the analysis with the Garching parametrization of the SN ν fluxes assuming the values for the initial ν spectra given in Tab. I. To understand the effect of varying pinching parameters let us first assume that the β_{ν_α} parameters are known. In Fig. 4 we represent by the dashed (solid) blue ellipses the regions allowed at 2σ (3σ) CL in the space spanned by $\langle E_{\bar{\nu}_e} \rangle - \langle E_{\nu_x} \rangle$ (left panel), $\langle E_{\bar{\nu}_e} \rangle - E_{\bar{\nu}_e}^{\text{tot}}$ (middle panel), and $\langle E_{\nu_x} \rangle - E_{\nu_x}^{\text{tot}}$ (right panel). In each panel, the best fit point is also indicated by a star, which of course reproduces the input value. It can be seen how we can determine $\langle E_{\bar{\nu}_e} \rangle$, $\langle E_{\nu_x} \rangle$, $E_{\bar{\nu}_e}^{\text{tot}}$, and $E_{\nu_x}^{\text{tot}}$ with an accuracy of roughly 2%, 4%, 15%, and 30%, respectively, at 3σ CL. These results are in good agreement with our previous work [20] apart from small differences due to different assumptions on the initial spectra and the detector (now with slightly smaller volume). It is remarkable that the non-vanishing mixing angle θ_{12} allows us to obtain information about ν_x flux parameters event though only $\bar{\nu}_e$'s are directly detected. This is a direct consequence of Eq. (7).

However, once we allow the pinching parameters β_{ν_α} to vary freely, the accuracy in the
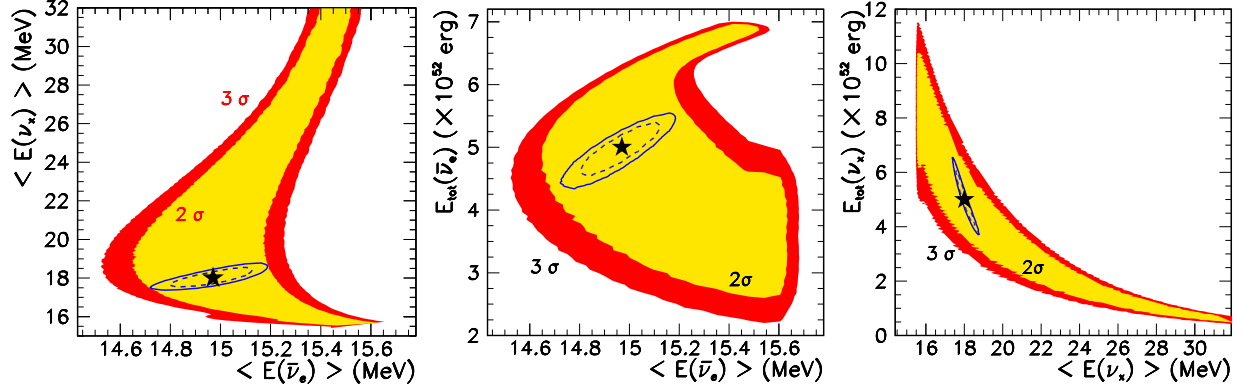
FIG. 4: Comparison between the 2σ CL and 3σ CL determination of the astrophysical parameters for the cases of fixed and free pinching parameters, displayed in terms of $\langle E_{\bar{\nu}_e}\rangle - \langle E_{\nu_x}\rangle$ (left panel), $\langle E_{\bar{\nu}_e}\rangle - E_{\bar{\nu}_e}^{\text{tot}}$ (middle panel), and $\langle E_{\nu_x}\rangle - E_{\nu_x}^{\text{tot}}$ (right panel). The solid and the dashed ellipses indicate the cases in which $\beta_{\bar{\nu}_e}$ and β_{ν_x} are fixed to $\beta_{\bar{\nu}_e} = 5$ and $\beta_{\nu_x} = 4$. The star represents the best-fit point, which, in this case, coincides with the input values. The constraint $\tau \equiv \langle E_{\nu_x}\rangle/\langle E_{\bar{\nu}_e}\rangle \geq 1$ has been imposed. The corresponding at 2σ CL and 3σ CL determinations for the case of free pinching parameters are denoted by the (dark/red) and (light/yellow) regions. See the text and Tab. I for more details.

determination of the flux parameters is significantly reduced. This is represented in Fig. 4 with shaded areas, yellow (light) and red (dark) corresponding to 2 and 3σ CL respectively. The striking consequence is the emergence of a *continuous parameter degeneracy*[4]: there is a continuum of allowed fit solutions. For definiteness, in what follows we make a very conservative assumption, $\langle E_{\bar{\nu}_x}\rangle \leq 32$ MeV. We find that this degeneracy affects $\bar{\nu}_e$ and ν_x flux parameter determination in a different way. For $\bar{\nu}_e$ the sensitivities to $\langle E_{\bar{\nu}_e}\rangle$ and $E_{\bar{\nu}_e}^{\text{tot}}$ are reduced to 4% and 50%, respectively, at 3σ CL. As can be seen in Fig. 4 for the case of ν_x, however, the effect is much more drastic. The region consisting of degenerate solutions forms a quasi one-dimensional strip extending mainly in the direction of ν_x SN flux parameters. This is a direct consequence of the different weights with which the original ν_α fluxes enter in the observed $\bar{\nu}_e$ flux: 70% from $\bar{\nu}_e$ and 30% from ν_x, see Eq. (7).

In order to shed more light on the nature of the degeneracy we present in Fig. 5 the allowed regions displayed in terms of various other combinations of the flux parameters. ¿From the last panel of Fig. 4 and the top left panel of Fig. 5 it can be inferred that the key of the continuous degeneracy lies on the possibility of increasing the pinching of $F^0_{\nu_x}$,

---

[4] Note that this degeneracy is quite different in nature from the (discrete) degeneracy one encounters in the determination of lepton mixing parameters in neutrino oscillation experiments [71, 72, 73].
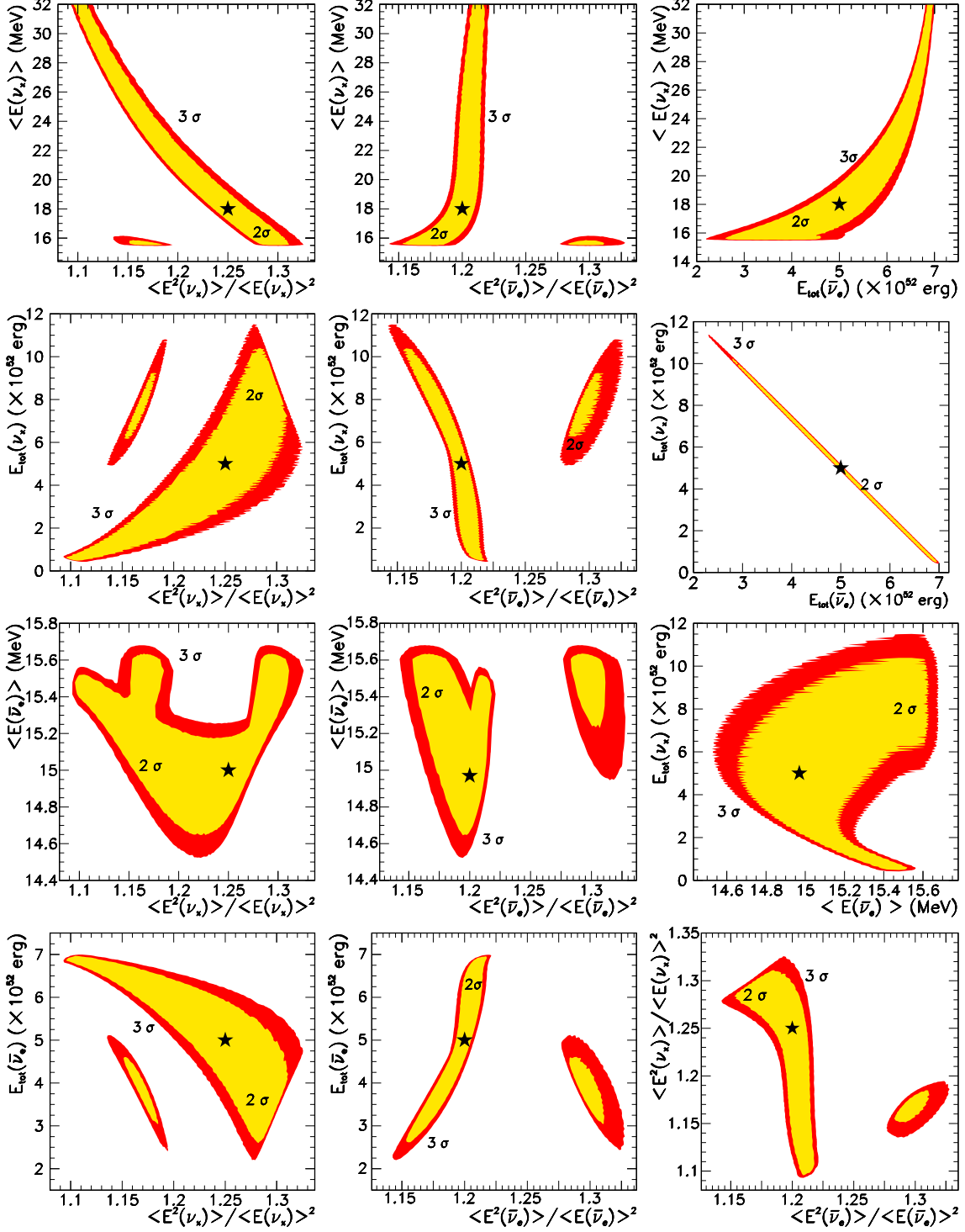
FIG. 5: Best-fit point (star) and 2σ CL and 3σ CL projections over the displayed parameters for free pinching parameters in the Garching parametrization.

i.e. larger β_{ν_x} and smaller p_{ν_x}. By requiring a stronger pinching of the ν_x flux, together with a larger value of $\langle E_{\nu_x} \rangle$ and a simultaneous reduction of $E_{\nu_x}^{\text{tot}}$ it is perfectly possible to mimic the behavior of observables defined with input values of $F_{\nu_x}^0$. In the bottom right panel one can see how the required variation of p_{ν_x} does not necessarily imply a significant

modification of the shape of the $\bar{\nu}_e$ flux. This feature can be seen for instance in the left panel of Fig. 1. In that example the *fake* spectra can be made surprisingly similar to the *true* one roughly by keeping the same original $F^0_{\bar{\nu}_e}$ parameters and changing $F^0_{\nu_x}$ following the previous recipe: a reduction of $E^{\text{tot}}_{\nu_x}$ together with an increase of β_{ν_x} and $\langle E_{\nu_x} \rangle$.

Another salient feature that can be observed in most of the panels of Fig. 5 is an island structure, i.e. the presence of a region separated from the main allowed region containing the best fit point. To understand the origin of such structure one has to realize that this region arises for larger values $p_{\bar{\nu}_e}$ and $\langle E_{\bar{\nu}_e} \rangle$ than the initial ones, and smaller p_{ν_x} and $\langle E_{\nu_x} \rangle$. This is related to the trivial degeneracy mentioned before, the extra solution obtained by interchanging the $\bar{\nu}_e$ and ν_x spectra. When we do not impose the condition $\langle E_{\nu_x} \rangle > \langle E_{\bar{\nu}_e} \rangle$, the allowed region has a "cross shape" because of the trivial degeneracy, namely the region with swapped parameters between $\bar{\nu}_e$ and ν_x is allowed. It appears to us that the island which is left over is a remnant of the swapped parameter region.

B. Robustness of the degeneracy

It is reasonable to ask whether the degeneracy is an artifact of the particular parametrization we employ, or an accidental consequence of the particular choice of the initial parameters. In order to answer the first question we performed the same exercise by using the pinched Fermi-Dirac parametrization, Eq. (1), both in the preparation of data, using the input values given in Tab. I, as well as in fitting them. As shown in Fig. 6 the shapes and the sizes of the allowed regions are very similar to those given in Figs. 4 and 5 (for brevity, we have shown our results only for 6 representative combinations out of 15, because the others are similar to previous plots). The continuous parameter degeneracy is also present for the same combination of ν_x parameters: strong pinching, large mean energies and small integrated luminosity. The main difference from the case with the Garching parametrization is the absence of the island structure.

In order to shed some light on the dependence of the results on the values of the initial neutrino fluxes we have redone the fit in the case of Garching data fitted by Garching distribution for $\langle E_{\nu_x} \rangle = 16.5$ and 20 MeV, which are presented in Figs. 7 and 8, respectively. One can see the shape of the allowed regions changes but the presence of the continuous degeneracy persists with a similar range of ν_x parameters. On the other hand, the size of the island region changes depending on the initial parameters considered. The more similar the initial $\bar{\nu}_e$ and ν_x spectra, the bigger the island. This is due to the fact that it is easier to interchange the role of the two flavors.

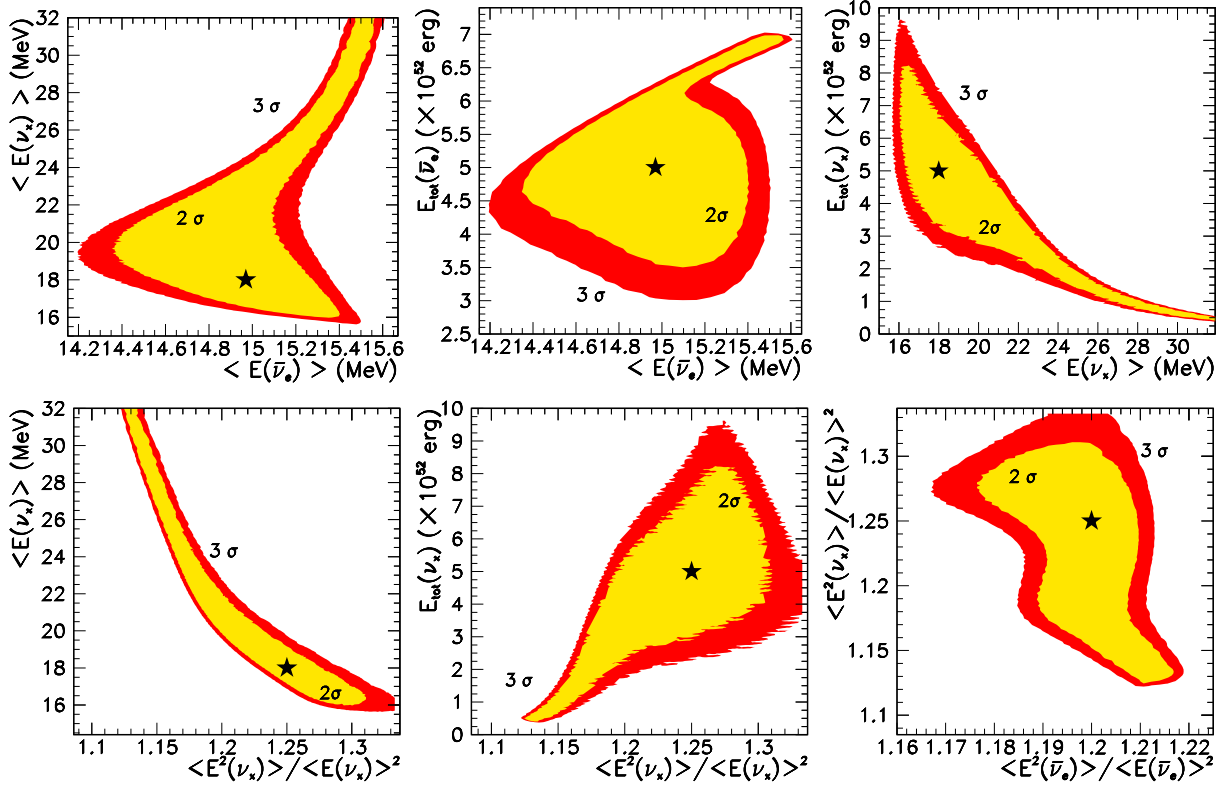For completeness we have also varied the number of energy bins used in the statistical

FIG. 6: Best-fit points (star) and 2σ CL and 3σ CL projections over the displayed parameters for free pinching parameters in the Fermi-Dirac parametrization. Here six representative combinations of fitting parameters were chosen, corresponding to the 3 panels in Fig. 4 and top 3 panels in Fig. 5.
.

analysis, but found no significant change in the result. We conclude then that the presence of the continuous degeneracy is a robust feature of the reconstruction analysis of supernova parameters.

C. Effect of uncertainties in the SN neutrino flux spectra

So far we have assumed in our analysis that we know the functional form of the supernova neutrino flux spectra prepared by the exploding star. Of course, this is *not* the case. What would be the effect of our ignorance of primordial SN neutrino flux spectra parametrization on the analysis? In order to gain some insight on this issue in this subsection we attempt a new procedure: to generate the data with a Fermi-Dirac distribution and to fit it assuming the Garching parametrization, and vice versa. This way we try to check not only whether it is possible to determine the flux parameters, but also its functional form.
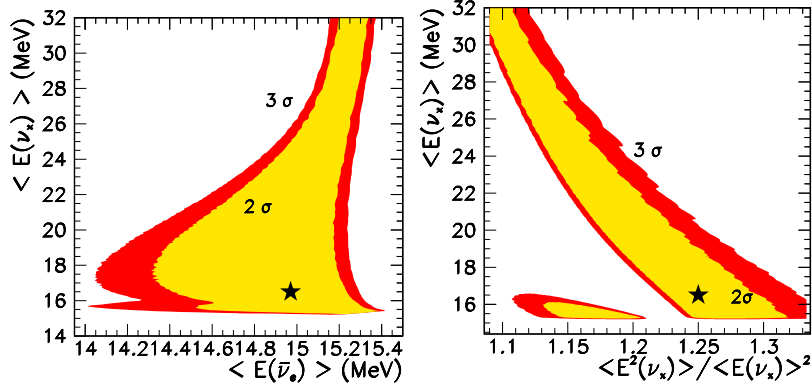
16

FIG. 7: Best-fit point (star) and allowed 2σ CL and 3σ CL projections over the displayed parameters for free pinching parameters in the Garching parametrization. Here we use as input the values given in Tab. I, except for $\langle E_{\nu_x} \rangle$, which is 16.5 MeV. Two fitting parameter combinations were selected: the left panel corresponds to the top left panel of Fig. 6 whereas the right one corresponds to the bottom left panel of the same figure.
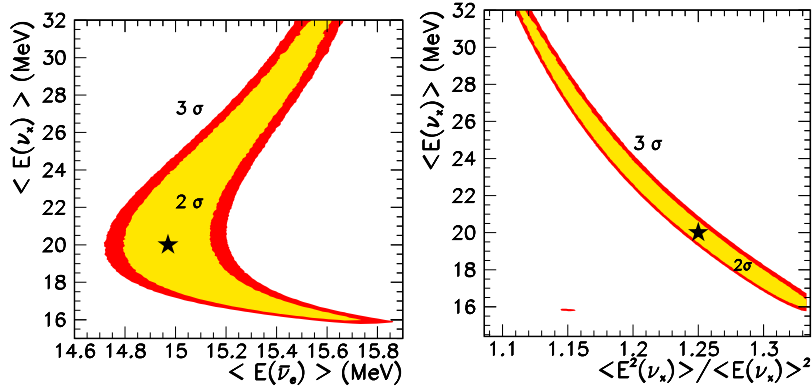

FIG. 8: Same as in Fig. 7 but for $\langle E_{\nu_x} \rangle = 20$ MeV.

The results of such a fit are presented in Fig. 9. In the left panels we show the allowed 2σ and 3σ CL contours assuming data generated with a Fermi-Dirac distribution, with input values given in Tab. I, and fitted with the Garching parametrization. First of all, one realizes that the shape of the contours are very similar to those presented in the previous sections, see e.g. Figs. 4 and 5. In particular, one finds the same one-dimensional correlations between the different parameters characterizing $F_{\nu_x}^0$. It is curious to note that the size of the allowed regions is smaller than in the previous figures. The second feature to point out is that the best-fit point does not coincide with the initial values assumed to generate the data. The χ^2 value obtained in the best-fit point is $\chi^2_{\text{bets}} = 5.29$[5].

---

[5] Notice, however, that these numbers have mild dependence on how fine is the mesh by which the parameter space is covered.
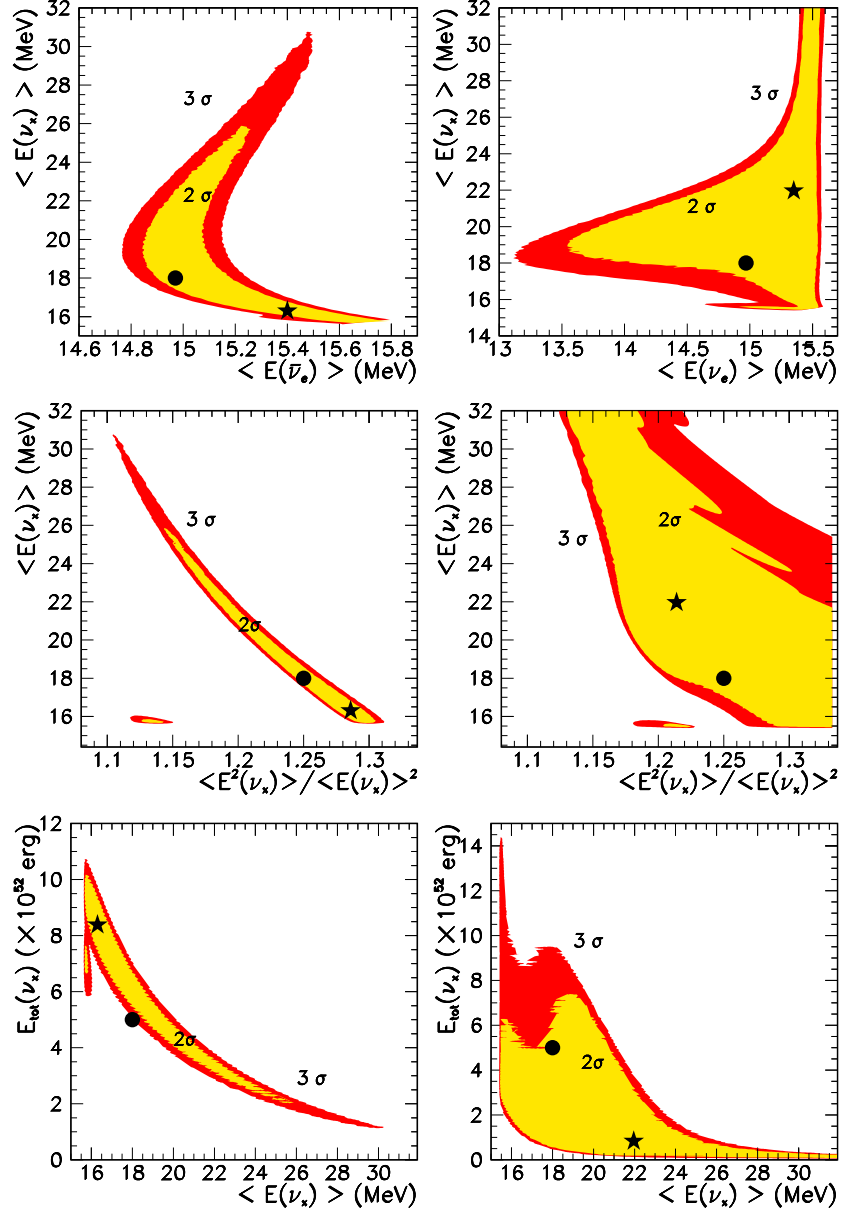
FIG. 9: Left panels: Allowed 2σ CL and 3σ CL contours assuming data generated with a Fermi-Dirac distribution and fitted with the Garching parametrization. Right panels: Allowed 2σ CL and 3σ CL contours assuming data generated with the Garching distribution and fitted using the Fermi-Dirac parametrization. The initial values are taken from Tab. I and are represented by a filled circle. The best fit points are shown with a star and have a value of $\chi^2_{\text{best}} = 5.29$ and 3.34 in the left and right panels, respectively.

In the right panels we show the same contours fixing the data with the Garching parametrization and carrying out the fit assuming a Fermi-Dirac distribution. One can still recognize roughly the same tendencies as in the previous case. However the contours

are much bigger. As far as the best fit point is concerned, it has a value of $\chi^2_{\text{bets}} = 3.34$, and as in the previous case it also does not coincide with the input values. These broad features indicate that Fermi-Dirac parametrization has somewhat higher *flexibility* than the Garching one, at least for the input values we used in this paper.

We note here that the results presented in Fig. 9 not only demonstrate the robustness of the degeneracy but also serve for providing some clues to answering the question of whether the SN neutrino observation can discriminate between different energy distribution of SN flux. The values of χ^2_{best} for both cases (input given by Garching parametrization fitted by Fermi Dirac one, and vice versa) are small compared to the number data points (bins), 85 bins. This implies that both distributions can fit equally well irrespective of the assumed input. Within our current procedure it seems rather difficult, by fitting only the observed data, to say which parametrization would describe better the SN spectra. We note that such a difficulty arises because the observed spectra are given by the superposition of the 2 spectra which is the origin of the degeneracy we found in this work. If the spectra were described only by the single spectrum by either Fermi-Dirac or Garching parametrization (hence no degeneracy) it would be possible to distinguish the functional form thanks to the huge statistics.

D.   Analytic understanding of correlations

Examining previous figures, e. g. Fig. 4, Fig. 5 and Fig. 6, one sees that they exhibit some intriguing correlations between the flux parameters. Let us now try to understand these features. We have seen in Fig. 1 that the degeneracy is present at the level of the fluxes arriving at the Earth, already before the detection process enters into the game. In particular, since our detection channel is the inverse beta decay, all the features observed in the fit should be encoded in the $\bar{\nu}_e$ flux at the Earth. For this reason let us consider the following quantities

$$E_{\text{ob}}^{\text{tot}} = \int E F_{\bar{\nu}_e} \mathrm{d}E, \qquad \langle E_{\text{ob}} \rangle = \frac{\int E F_{\bar{\nu}_e} \mathrm{d}E}{\int F_{\bar{\nu}_e} \mathrm{d}E}, \qquad \langle E_{\text{ob}}^2 \rangle = \frac{\int E^2 F_{\bar{\nu}_e} \mathrm{d}E}{\int F_{\bar{\nu}_e} \mathrm{d}E} \qquad (8)$$

These functionals are determined in terms of the energy spectrum of $F_{\bar{\nu}_e}$ at the Earth.

Of the six fit parameters we have, one notices from the previous Figures that the range of variation of two of them is rather narrow, namely $\langle E_{\bar{\nu}_e} \rangle$ and $p_{\bar{\nu}_e}$. Hence in order to understand the nature of the correlations we need only the 4 remaining "effective" parameters. Using Eq. (8) and requiring these quantities to be equal to the observed (input) values, we see that these 4 parameters are correlated, and one can choose to express the dependence of $E_{\bar{\nu}_e}^{\text{tot}}$, $\langle E_{\nu_x} \rangle$, and p_{ν_x}, in terms of one, e.g. $E_{\nu_x}^{\text{tot}}$.

Taking into account the relation in Eq. (7), $E_{\mathrm{ob}}^{\mathrm{tot}}$ is trivially obtained by our assumption on the initial values of the total energies $E_{\bar{\nu}_e}^{\mathrm{tot}} = E_{\nu_x}^{\mathrm{tot}} = 5 \times 10^{52}$ erg, see Tab. I, as

$$E_{\mathrm{ob}}^{\mathrm{tot}} = c_{12}^2 E_{\bar{\nu}_e}^{\mathrm{tot}} + s_{12}^2 E_{\nu_x}^{\mathrm{tot}} = 5 \times 10^{52} \text{ erg}, \tag{9}$$

where c_{12}^2 and s_{12}^2 stand for $\cos^2 \theta_{12}$ and $\sin^2 \theta_{12}$, respectively. If we now fix $E_{\mathrm{ob}}^{\mathrm{tot}}$ to this value and let $E_{\bar{\nu}_e}^{\mathrm{tot}}$ and $E_{\nu_x}^{\mathrm{tot}}$ freely vary we get, after substituting the value of θ_{12} the following trivial relation

$$E_{\bar{\nu}_e}^{\mathrm{tot}} = 1.43 E_{\mathrm{ob}}^{\mathrm{tot}} - 0.43 E_{\nu_x}^{\mathrm{tot}}, \tag{10}$$

which explains the anti-correlation found between $E_{\bar{\nu}_e}^{\mathrm{tot}}$ and $E_{\nu_x}^{\mathrm{tot}}$ in the right panel in the second row of Fig. 5.

The approximate quasi one-dimensional correlation is displayed in Fig. 10. In the figure, we plot $\alpha = \alpha(E_{\nu_x}^{\mathrm{tot}})$, where α represents $E_{\bar{\nu}_e}^{\mathrm{tot}}$, $\langle E_{\bar{\nu}_e} \rangle$, $\langle E_{\nu_x} \rangle$, $p_{\bar{\nu}_e}$, and p_{ν_x}. It is defined as the value of α that minimizes $\chi^2(\alpha, E_{\nu_x}^{\mathrm{tot}})$ for a given $E_{\nu_x}^{\mathrm{tot}}$. This plot illustrates how the different parameters adjust themselves when $E_{\nu_x}^{\mathrm{tot}}$ is varied so that the new set of parameters fits equally well. Together with $\alpha(E_{\nu_x}^{\mathrm{tot}})$ we show the analytical expression obtained by requiring the quantities defined in Eq. (8) to be equal to the observed (input) values.

In the top panel of Fig. 10 we can see how the expected anti-correlation for $\alpha = E_{\bar{\nu}_e}^{\mathrm{tot}}$ (see the right panel in the second row in Fig. 5) completely agrees with the analytical expression 10.

Let us now consider the mean energy of the $\bar{\nu}_e$ arriving at the Earth. According to the values assumed for the input parameters describing the flux one expects,

$$\langle E_{\mathrm{ob}} \rangle = \frac{E_{\mathrm{ob}}^{\mathrm{tot}}}{c_{12}^2 E_{\bar{\nu}_e}^{\mathrm{tot}} / \langle E_{\bar{\nu}_e} \rangle + s_{12}^2 E_{\nu_x}^{\mathrm{tot}} / \langle E_{\nu_x} \rangle} = 15.79 \text{ MeV}. \tag{11}$$

We can now proceed as before and rewrite $\langle E_{\nu_x} \rangle$ in terms of $E_{\nu_x}^{\mathrm{tot}}$ taking into account Eq. (9):

$$\langle E_{\nu_x} \rangle = \frac{s_{12}^2 E_{\nu_x}^{\mathrm{tot}}}{s_{12}^2 E_{\nu_x}^{\mathrm{tot}} - E_{\mathrm{ob}}^{\mathrm{tot}} (1 - \langle E_{\bar{\nu}_e} \rangle / \langle E_{\mathrm{ob}} \rangle)} \langle E_{\bar{\nu}_e} \rangle = 15 \frac{E_{\nu_x}^{\mathrm{tot}}}{E_{\nu_x}^{\mathrm{tot}} - 8.34 \times 10^{51} \text{ erg}} \text{ MeV}. \tag{12}$$

where in the last step we have assumed that $\langle E_{\bar{\nu}_e} \rangle$ and $\langle E_{\mathrm{ob}} \rangle$ are constant and equal to 15 MeV and 15.79 MeV, respectively. Under this assumption we expect that $\langle E_{\nu_x} \rangle$ decreases for large values of $E_{\nu_x}^{\mathrm{tot}}$. This behavior can be clearly seen in the right panel in Fig. 4 as well as in the middle panel of Fig. 10 (see the red solid curve). Moreover, from the same panel one sees that the assumption of constant $\langle E_{\bar{\nu}_e} \rangle$ (blue curve) is justified when compared to the variation of $\langle E_{\nu_x} \rangle$ (red curve). However, this assumption is not perfect and therefore the observed variation of $\langle E_{\nu_x} \rangle$ and the analytical prediction from Eq. 12 (black curve) do not coincide.
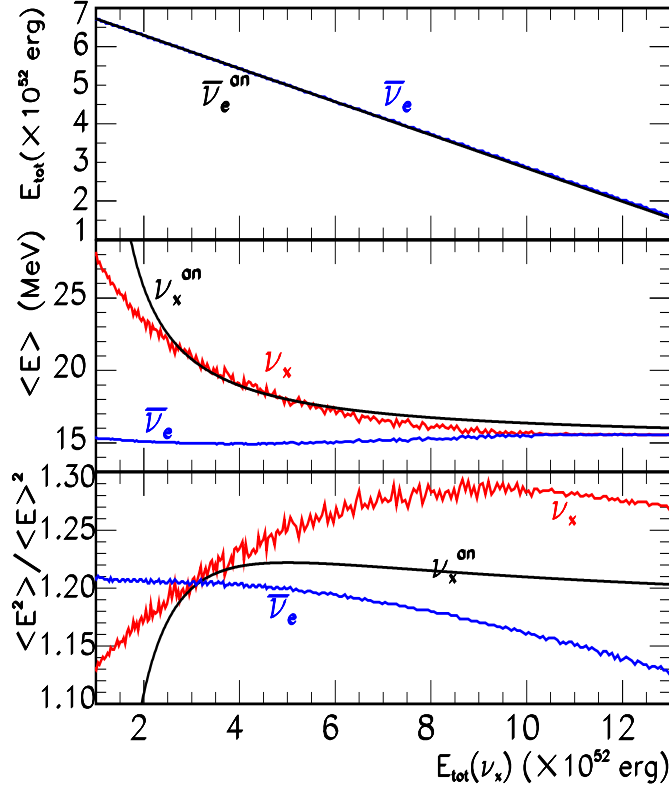
FIG. 10: Various quantities are plotted as a function of $E_{\nu_x}^{\text{tot}}$, in blue and red for $\bar{\nu}_e$ and ν_x, respectively. The total energy $E_{\bar{\nu}_e}^{\text{tot}}$ is shown in the top panel, the average energies $\langle E \rangle$ in the middle panel, and the width parameters $\langle E^2 \rangle / \langle E \rangle^2$ in the bottom one. The analytical values predicted in Eqs. (10, 12, 14) are also plotted in black. See text for details.

Now we analyze the second moment of the flux,

$$\langle E_{\text{ob}}^2 \rangle = \frac{c_{12}^2 E_{\bar{\nu}_e}^{\text{tot}} \langle E_{\bar{\nu}_e} \rangle p_{\bar{\nu}_e} + s_{12}^2 E_{\nu_x}^{\text{tot}} \langle E_{\nu_x} \rangle p_{\nu_x}}{c_{12}^2 E_{\bar{\nu}_e}^{\text{tot}} / \langle E_{\bar{\nu}_e} \rangle + s_{12}^2 E_{\nu_x}^{\text{tot}} / \langle E_{\nu_x} \rangle} = 305.53 \text{ MeV}^2 \,. \tag{13}$$

Taking into account Eqs. (9), (11) and (13) we can express p_{ν_x} in terms of $\langle E_{\nu_x} \rangle$:

$$p_{\nu_x} = \frac{\langle E_{\text{ob}}^2 \rangle}{\langle E_{\bar{\nu}_e} \rangle \langle E_{\nu_x} \rangle} \left\{ \left(1 - \frac{\langle E_{\bar{\nu}_e} \rangle}{\langle E_{\nu_x} \rangle} \right) \frac{\langle E_{\bar{\nu}_e} \rangle / \langle E_{\text{ob}} \rangle - \langle E_{\bar{\nu}_e}^2 \rangle / \langle E_{\text{ob}}^2 \rangle}{1 - \langle E_{\bar{\nu}_e} \rangle / \langle E_{\text{ob}} \rangle} + \frac{\langle E_{\bar{\nu}_e}^2 \rangle}{\langle E_{\text{ob}}^2 \rangle} \right\} \,. \tag{14}$$

Analogously to the previous case we can require $\langle E_{\text{ob}}^2 \rangle$ and $p_{\bar{\nu}_e}$ to be constant. Then, from this expression one can see how as $\langle E_{\nu_x} \rangle$ increases the ν_x spectrum has to become more pinched in order to keep the same *shape*. Taking into account that $\langle E_{\nu_x} \rangle$ and $E_{\nu_x}^{\text{tot}}$ are anti-correlated one expects a *positive* correlation between p_{ν_x} and $E_{\nu_x}^{\text{tot}}$. This is exactly what is seen in Figs. 5 (left panel in the second row) and in the bottom panel of Fig. 10 (red curve). In the latter figure we see how this argument is mainly qualitative, since $p_{\bar{\nu}_e}$ is not constant over the whole range of the $E_{\nu_x}^{\text{tot}}$ considered. Actually, when comparing this result

21

with the analytical condition (14) one realizes that this qualitative argument only applies for a definite range of $E_{\nu_x}^{\text{tot}}$.

V.   RESOLVING THE DEGENERACY?

Once the presence and robustness of the degeneracy have been established, the next step is to point out strategies to solve the problem. Here we comment on three possible directions that could be followed.

First from the theory side we note that a better understanding of the neutrino flux formation would narrow down the range of values that the flux parameters could take. In particular we have seen in Fig. 5 how our knowledge of the pinching parameter can play an essential role in reducing the uncertainties on the traditionally considered parameters $\langle E_{\nu_\alpha}\rangle$ and $E_{\nu_\alpha}^{\text{tot}}$.

From an experimental point of view one may correctly argue that the degeneracy we have pointed out is an artifact of our treatment, which uses only the $\bar{\nu}_e$ absorption reaction. The obvious way of resolving such a degeneracy would be to include other reactions into the analysis, such as neutrino elastic scattering off electrons, or CC and NC reactions with oxygen. Indeed, the quasi one-dimensional nature of the degeneracy we found would suggest that it would be lifted by adding an extra high statistics observable, independent of inverse beta decay.

However, the situation in our case is quite different. To understand why, one must recall the following crucial fact. In order to include the previous reactions one must also include ν_e into the analysis. As a result instead of the six supernova neutrino flux parameters used in our fitting procedure we would need nine. Since the number of events due to the above reactions is more than one order of magnitude less than those coming from the $\bar{\nu}_e$ absorption reaction, it is not obvious at all that, by adding these other reactions one will indeed resolve the degeneracy we have uncovered.

If the degeneracy cannot be resolved simply by using water Cherenkov detectors one must think of possible alternative detectors to combine with. For example the situation might improve either by: (1) adding detectors with better sensitivity on ν_x parameters, or (2) adding detectors sensitive to ν_e. Good candidates in the current and near future experiments which can contribute towards these goals would be Borexino [74], KamLAND (in its future solar neutrino observation phase) [75] and HALO project [76]. The former 2 detectors will be able to observe proton recoil in νp elastic scattering in a liquid scintillator [77]. We stress that this would provide a unique opportunity to obtain the spectrum information of NC reactions which should be very important in resolving the degeneracy. The latter, on the

other hand, would have capabilities to detect ν_x and ν_e through the NC and the CC reactions on lead. With regard to the possibility (2) above it would be interesting to consider a high statistics measurement of ν_e events in a liquid argon neutrino detector through the charged current absorption of ν_e by ^{40}Ar [57]. As can be inferred from Eq. (7), the dependence of the ν_e flux at the Earth on the original $F^0_{\nu_e}$ and $F^0_{\nu_x}$ is different from that of antineutrinos. In particular for *large θ_{13}* the following condition holds

$$F_{\nu_e} = s^2_{13} F^0_{\nu_e} + c^2_{13} F^0_{\nu_x} \approx F^0_{\nu_x} \,. \tag{15}$$

Therefore, one could hope that this fact could break the degeneracy expected in water Cherenkov detectors. Nevertheless the possibility of distinguishing between the ν_e and $\bar{\nu}_e$ signals is in any case non-trivial. Therefore, a realistic nine-dimensional parameter analysis taking into account all neutrino flavors is outside the scope of this paper but should be taken up as a next step.

VI.   CONCLUDING REMARKS

In this paper, we have reexamined the possibility of reconstructing the initial fluxes of the neutrinos emitted in a future galactic core-collapse supernova by using a Megaton-sized water Cherenkov detector.

The three parameters that are usually considered to characterize the non-thermal supernova neutrino flux are the average and total energies of each species, and the so-called pinching parameter. The latter is connected to the second moment of the distribution function and modulates its shape. Due to the current uncertainty on its precise value, we have included the pinching parameter as a fit parameter, in contrast to previous works where only the average and total energies were considered.

In order to illustrate our results we have considered the following scenario. First of all, from all reactions giving rise to the neutrino signal in a water Cherenkov detector we have concentrated on the inverse beta decay, $\bar{\nu}_e + p \rightarrow e^+ + n$, which is by far the most important one. Therefore, our setting is sensitive only to the anti-neutrino fluxes at terrestrial detectors.

As far as the neutrino properties are concerned, we have focused on the case of normal mass hierarchy neutrinos, neglecting also any non-standard neutrino interactions which could affect neutrino propagation in an important way. Such well-defined scenario is much less affected by uncertainties due to neutrino self-interaction in the inner layers or the distortion of the matter density due to the shock wave passage.

On the other hand the $\bar{\nu}_e$ flux arriving at the Earth is in this case a strong mixture of the initial $\bar{\nu}_e$ and ν_x. Therefore the detected $\bar{\nu}_e$ flux would provide us with information not only

about $\bar{\nu}_e$ but also ν_x. Under these assumptions we performed a χ^2 analysis on artificially generated data.

We found that the inclusion of the pinching parameter in the fit analysis has a drastic consequence: the appearance of a continuous degeneracy in the determination of the ν_x flux parameters. This degeneracy is quite robust, as it persists irrespective of the parametrization taken for the neutrino distributions. This makes very difficult a complete determination of the different parameters characterizing the ν_x flux using the inverse beta decay events, even in the case of a Megaton water Cherenkov detector.

The solution to this degeneracy must come from a better understanding of the neutrino spectra formation, as well as an optimization of the information provided by the complementary neutrino reactions involved not only in water Cherenkov detectors, but also in alternative detector techniques.

Note added: After completion of our work we became aware of the paper [78], which was in fact triggered by previous private communications with us. Their analysis includes other reactions available in water Cherenkov detectors. However, their results indicate that the addition of these channels is not enough to fully resolve the degeneracy pointed out here.

[1] KAMIOKANDE-II collaboration, K. Hirata *et al.*, Phys. Rev. Lett. **58**, 1490 (1987).

[2] K. S. Hirata *et al.*, Phys. Rev. D **38**, 448 (1988).

[3] IMB collaboration, R. M. Bionta *et al.*, Phys. Rev. Lett. **58**, 1494 (1987).

[4] M. Rampp and H. T. Janka, Astrophys. J. **539**, L33 (2000) [astro-ph/0005438].

[5] A. Mezzacappa *et al.*, Phys. Rev. Lett. **86**, 1935 (2001) [astro-ph/0005366].

[6] T. A. Thompson, A. Burrows, and P. A. Pinto, Astrophys. J. **592**, 434 (2003) [astro-ph/0211194].

[7] M. Liebendoerfer *et al.*, Phys. Rev. **D63**, 103004 (2001) [astro-ph/0006418].

[8] R. Buras, H.-T. Janka, M. Rampp, and K. Kifonidis, Astronomy and Astrophysics **457**, 281 (2006).

[9] S. W. Bruenn *et al.*, J. Phys. Conf. Ser. **46**, 393 (2006) [arXiv:0709.0537 [astro-ph]].

[10] A. Burrows, E. Livne, L. Dessart, C. Ott, and J. Murphy, Astrophys. J. **640**, 878 (2006) [astro-ph/0510687].

[11] C. Y. Cardall, Nucl. Phys. Proc. Suppl. **168**, 96 (2007) [astro-ph/0703334].

[12] J. F. Beacom, Talk at Neutrino Workshop at Institute for Nuclear Theory, Seattle, Washington, September 21-23, 2000; and H. Minakata, talk at "Frontiers in Particle Astrophysics and Cosmology" EuroConference on Neutrinos in the Universe, Lenggries, Germany, September 29 - October 4, 2001.

[13] G. G. Raffelt, astro-ph/0701677.

[14] KamLAND collaboration, T. Araki *et al.*, Phys. Rev. Lett. **94**, 081801 (2005).

[15] SNO, B. Aharmim *et al.*, Phys. Rev. **C72**, 055502 (2005), nucl-ex/0502021.

[16] M. Maltoni, T. Schwetz, M. A. Tortola, and J. W. F. Valle, New J. Phys. **6**, 122 (2004), version 6 of the arXiv, hep-ph/0405172, provides updated results; previous works by other groups as well as the relevant experimental references are given therein.

[17] T. Schwetz, M. Tortola and J. W. F. Valle, New J. Phys. **10**, 113011 (2008).

[18] A. Burrows, D. Klein, and R. Gandhi, Phys. Rev. **D45**, 3361 (1992).

[19] K. Scholberg, astro-ph/0701081.

[20] H. Minakata, H. Nunokawa, R. Tomàs, and J. W. F. Valle, Phys. Lett. **B542**, 239 (2002) [hep-ph/0112160].

[21] V. Barger, D. Marfatia, and B. P. Wood, Phys. Lett. **B547**, 37 (2002) [hep-ph/0112125].

[22] H. Janka and W. Hillebrandt, Astronomy and Astrophysics **224**, 49 (1989).

[23] A. Mirizzi and G. G. Raffelt, Phys. Rev. **D72**, 063001 (2005) [astro-ph/0508612].

[24] S. K. Okumura, talk given at Workshop on Next Generation Nucleon Decay and Neutrino Detectors 2007 (NNN07) Hamamatsu, Japan, October 2 - 5, 2007, http://www-rccn.icrr.u-tokyo.ac.jp/NNN07/.

[25] UNO web-page at Stonybrook http://superk.physics.sunysb.edu/nngroup/uno/main.html.

[26] A. de Bellefon *et al.*, hep-ex/0607026.

[27] G. G. Raffelt, Astrophys. J. **561**, 890 (2001) [astro-ph/0105250].

[28] R. Buras, H.-T. Janka, M. T. Keil, G. G. Raffelt, and M. Rampp, Astrophys. J. **587**, 320 (2003) [astro-ph/0205006].

[29] G. G. Raffelt, M. T. Keil, R. Buras, H.-T. Janka, and M. Rampp, astro-ph/0303226.

[30] M. T. Keil, G. G. Raffelt and H. T. Janka, Astrophys. J. **590**, 971 (2003) [arXiv:astro-ph/0208035].

[31] A. Mezzacappa, Ann. Rev. Nucl. Part. Sci. **55**, 467 (2005).

[32] M. T. Keil, astro-ph/0308228.

[33] H. T. Janka, B. Mueller, F. S. Kitaura and R. Buras, arXiv:0712.4237 [astro-ph].

[34] H. Duan, G. M. Fuller, J. Carlson and Y. Z. Qian, Phys. Rev. Lett. **100**, 021101 (2008) [arXiv:0710.1271 [astro-ph]].

[35] H. Duan, G. M. Fuller, and Y.-Z. Qian, Phys. Rev. **D74**, 123004 (2006) [astro-ph/0511275].

[36] H. Duan, G. M. Fuller, J. Carlson, and Y.-Z. Qian, Phys. Rev. **D74**, 105014 (2006) [astro-ph/0606616].

[37] H. Duan, G. M. Fuller, J. Carlson, and Y.-Z. Qian, Phys. Rev. Lett. **97**, 241101 (2006) [astro-ph/0608050].

[38] S. Hannestad, G. G. Raffelt, G. Sigl, and Y. Y. Y. Wong, Phys. Rev. **D74**, 105010 (2006) [astro-ph/0608695].

[39] G. G. Raffelt and A. Y. Smirnov, Phys. Rev. **D76**, 081301 (2007) [arXiv:0705.1830 [hep-ph]].

[40] A. Esteban-Pretel, S. Pastor, R. Tomàs, G. G. Raffelt, and G. Sigl, Phys. Rev. **D76**, 125018 (2007) [arXiv:0706.2498 [astro-ph]].

[41] H. Duan, G. M. Fuller, J. Carlson, and Y.-Q. Zhong, Phys. Rev. Lett. **99**, 241802 (2007) [arXiv:0707.0290 [astro-ph]].

[42] G. L. Fogli, E. Lisi, A. Marrone and A. Mirizzi, JCAP **0712**, 010 (2007) [arXiv:0707.1998 [hep-ph]].

[43] A. Esteban-Pretel, S. Pastor, R. Tomàs, G. G. Raffelt and G. Sigl, Phys. Rev. D **77**, 065024 (2008) [arXiv:0712.1137 [astro-ph]].

[44] B. Dasgupta and A. Dighe, arXiv:0712.3798 [hep-ph].

[45] L. Wolfenstein, Phys. Rev. D **17**, 2369 (1978).

[46] S. P. Mikheev and A. Y. Smirnov, Sov. J. Nucl. Phys. **42**, 913 (1985)[Yad. Fiz. **42**, 1441 (1985)].

[47] T.-K. Kuo and J. T. Pantaleone, Rev. Mod. Phys. **61**, 937 (1989).

[48] A. S. Dighe and A. Y. Smirnov, Phys. Rev. **D62**, 033007 (2000) [hep-ph/9907423].

[49] H. Minakata and H. Nunokawa, Phys. Lett. **B504**, 301 (2001) [hep-ph/0010240].

[50] K. Takahashi and K. Sato, Prog. Theor. Phys. **109**, 919 (2003) [hep-ph/0205070].

[51] C. Lunardini and A. Y. Smirnov, JCAP **0306**, 009 (2003) [hep-ph/0302033].

[52] A. S. Dighe, M. T. Keil, and G. G. Raffelt, JCAP **0306**, 005 (2003) [hep-ph/0303210].

[53] A. S. Dighe, M. T. Keil, and G. G. Raffelt, JCAP **0306**, 006 (2003) [hep-ph/0304150].

[54] A. S. Dighe, M. Kachelrieß, G. G. Raffelt, and R. Tomàs, JCAP **0401**, 004 (2004) [hep-ph/0311172].

[55] V. Barger, P. Huber, and D. Marfatia, Phys. Lett. **B617**, 167 (2005) [hep-ph/0501184].

[56] S. Skadhauge and R. Zukanovich Funchal, JCAP **0704**, 014 (2007) [hep-ph/0611194].

[57] I. Gil-Botella and A. Rubbia, JCAP **0408**, 001 (2004) [hep-ph/0404151].

[58] P. Vogel and J. F. Beacom, Phys. Rev. **D60**, 053003 (1999) [hep-ph/9903554].

[59] A. Strumia and F. Vissani, Phys. Lett. **B564**, 42 (2003) [astro-ph/0302055].

[60] J. Hosaka *et al.* [Super-Kamkiokande Collaboration], Phys. Rev. D **73**, 112001 (2006) [arXiv:hep-ex/0508053].

[61] R. C. Schirato and G. M. Fuller, astro-ph/0205390.

[62] G. L. Fogli, E. Lisi, D. Montanino, and A. Mirizzi, Phys. Rev. **D68**, 033005 (2003) [hep-ph/0304056].

[63] R. Tomàs, M. Kachelrieß, G. Raffelt, A. Dighe, H. T. Janka and L. Scheck, JCAP **0409**, 015 (2004) [astro-ph/0407132].

[64] G. L. Fogli, E. Lisi, A. Mirizzi, and D. Montanino, JCAP **0504**, 002 (2005) [hep-ph/0412046].

[65] G. L. Fogli, E. Lisi, A. Mirizzi, and D. Montanino, JCAP **0606**, 012 (2006) [hep-ph/0603033].

[66] A. Friedland and A. Gruzinov, arXiv:astro-ph/0607244.

[67] J. P. Kneller, G. C. McLaughlin and J. Brockman, Phys. Rev. D **77**, 045023 (2008) [arXiv:0705.3835 [astro-ph]].

[68] B. Dasgupta and A. Dighe, Phys. Rev. D **75**, 093002 (2007) [arXiv:hep-ph/0510219].

[69] J. W. F. Valle, Phys. Lett. **B199**, 432 (1987). H. Nunokawa, Y. Z. Qian, A. Rossi, and J. W. F. Valle, Phys. Rev. **D54**, 4356 (1996) [hep-ph/9605301.

[70] A. Esteban-Pretel, R. Tomàs and J. W. F. Valle, Phys. Rev. D **76**, 053001 (2007) [arXiv:0704.0032 [hep-ph]].

[71] J. Burguet-Castell, M. B. Gavela, J. J. Gomez-Cadenas, P. Hernandez, and O. Mena, Nucl. Phys. **B608**, 301 (2001) [hep-ph/0103258].

[72] H. Minakata and H. Nunokawa, JHEP **10**, 001 (2001) [hep-ph/0108085].

[73] G. L. Fogli and E. Lisi, Phys. Rev. **D54**, 3667 (1996) [hep-ph/9604415].

[74] L. Cadonati, F. P. Calaprice and M. C. Chen, Astropart. Phys. **16**, 361 (2002) [arXiv:hep-ph/0012082].

[75] F. Suekane [KamLAND Collaboration], Prog. Part. Nucl. Phys. **57**, 106 (2006).

[76] C. Virtue, http://snolab2007.snolab.ca/snolab2007-programme.html

[77] J. F. Beacom, W. M. Farr, and P. Vogel, Phys. Rev. **D66**, 033001 (2002) [hep-ph/0205220].

[78] S. Skadhauge and R. Z. Funchal, arXiv:0802.1177 [hep-ph].